Numerical Investigation on CO_2 Absorbed in Aqueous *N*-Methyldiethanolamine + Piperazine

Jicai Huang
Key Laboratory of Cryogenics, Technical Inst. of Physics and Chemistry, Chinese Academy of Sciences, Beijing 100190, China

Division of Fuel Cell & Battery, Dalian National Laboratory for Clean Energy, Dalian Inst. of Chemical Physics, Chinese Academy of Sciences, Dalian 116023, China

Maoqiong Gong, Zhaohu Sun, Xueqiang Dong, Jun Shen, and Jianfeng Wu
Key Laboratory of Cryogenics, Technical Inst. of Physics and Chemistry, Chinese Academy of Sciences, Beijing 100190, China

DOI 10.1002/aic.15590
Published online November 24, 2016 in Wiley Online Library (wileyonlinelibrary.com)

A multiphase and multicomponent mass transfer model of CO_2 absorbed in aqueous N-methyldiethanolamine and piperazine (PZ) was built in the study. In the model, a simple method of mass transfer between phases was proposed. Besides, the hydrodynamics, thermodynamics, and complex reversible chemical reaction were considered simultaneously. The model was validated by comparing with the previous experimental data which showed that simulated results can represent the experimental data with reasonable accuracy. Based on the model, the effects of gas velocity, liquid load and CO_2 loading on the absorption rate, and enhancement factor were analyzed. Model results showed that the enhancement factor increased with a rising gas velocity while decreased with a rising liquid load or CO_2 loading. The change of enhancement factor with CO_2 loading was similar to that of equilibrium concentration of PZ which indicated that PZ was significant to the absorption process. Furthermore, the distributions of specie concentrations were discussed in detail. © 2016 American Institute of Chemical Engineers *AIChE J*, 63: 2386–2393, 2017
Keywords: chemical absorption, computational fluid dynamics, carbon dioxide, N-methyldiethanolamine, piperazine

Introduction

Aqueous amine solutions are widely used to remove acid gases such as CO_2 and H_2S from natural gas, power plant flue gas, synthetic gas, and refinery off gas.[1] One of the most commonly used absorbents is piperazine (PZ) activated *N*-methyldiethanolamine (MDEA).[2–4] Such absorption processes are usually accompanied by the chemical reaction in the liquid phase of gas-liquid contactor. To accurately design the separation process and equipment, it is necessary to build a comprehensive model that can describe the mass transfer phenomenon. To build such a model, there are mainly three aspects should be included. First, the hydrodynamic parameters such as the gas and liquid loads, velocity profile in the phase layer, and contactor structure. Second, the thermodynamic equilibrium condition which is used to calculate the driving force of multiphase mass transfer and species concentration in the liquid phase. Last, the rate consideration which includes convection-diffusion mass transfer in both of the phases and the chemical reaction kinetics.

During the last decades, the problem of gas absorption with chemical reaction has been extensively studied based on the two film theory,[5] the penetration theory,[6] the surface renewal theory,[7] and the film-penetration theory.[8] For the turbulent flow, a more realistic method is the eddy diffusivity theory in which the diffusion coefficient is revised to allow for the effect of turbulent.[9] Glasscock and Rochelle[10] compared the performances of these theories by the case of CO_2 absorbed in the aqueous MDEA. The result showed that eddy diffusivity theory had an excellent approximation to the surface renewal theory, and was generally more accurate than the film theory. Based on the eddy diffusivity theory, Bishnoi[11] built a rigorous one-dimensional model of CO_2 absorbed in the aqueous MDEA and PZ. Model results represented the experimental absorption rate obtained by a wetted wall column with reasonable accuracy, providing that the interfacial CO_2 pressure was given appropriately. However, the value in the model was determined by the experiment which indicated that the model tended to check the experimental operation rather than predict. Unlike the previous model, Samanta and Bandyopadhyay[12] developed a transient model for the absorption process.

Although the absorption models aforementioned[10–12] consider the rate and thermodynamic conditions, the hydrodynamic parameter which is crucial to the absorption process with finite liquid thickness is not included in detail.[13] Besides, mass transfer in the gas phase is not considered in these models. To represent the reality and build a completed model, it is necessary to consider all of these factors. Actually, the investigations on chemical absorption in a liquid layer with finite thickness and different flow patterns have been extensively conducted for a long time. For the laminar flow with half-parabolic velocity profile, analytical solutions have been

Correspondence concerning this article should be addressed to Z. Sun at zhsun@mail.ipc.ac.cn.

obtained for chemical absorption with zero-order reaction[14,15] and first-order reaction.[16,17] Numerical analyses have been performed for the cases with instantaneous reaction[18,19] and second-order reaction.[20,21] Similar works have been done for the plug flow[13,22] and turbulent flow.[23,24] However, these studies are mainly focused on the simple reaction, and few researches have been conducted for a reversible reaction considering the hydrodynamic parameters at the same time. With the development of computational fluid dynamics (CFD) theory and computer technology, it is possible to model flow behavior in the complex structure, and the method is potential to be extended to model mass transfer in the phase layer with finite thickness.[25–27] Recently, the CFD technology has been used to model the mass transfer with first-order reaction.[28] Unfortunately, mass transfer with multiple reactions, especially for instance with reversible reaction, seems more difficult to implement in the CFD software and is modeled by introducing an enhancement factor which is the ratio of absorption rate with and without chemical reaction.[29]

The industrial process of CO_2 absorbed in aqueous MDEA and PZ is mainly characterized by the three aspects. First, the liquid spray density is generally low resulting from low CO_2 composition in the gas and high efficiency of the absorbent. For the reason, the liquid layer is thin on the packing, and it is important to consider the hydrodynamics in the mass transfer model. Besides, to investigate the effects of equipment structure, gas, and liquid loads on the absorption process, the hydrodynamics of both phases should be included. Second, the thermodynamics for the system is complex. Since the reactions of CO_2 and mixed solvent lead to considerable species which have effect on the driving force of mass transfer, a rigorous thermodynamic model should be adopted. Last, it includes multiple reversible reactions. Some of them are assumed to be kinetically controlled while others are always considered to be in chemical equilibrium.[11] All the three aspects are important and should be included in a completed model. The previous studies either not pay enough attention to the hydrodynamics or the complex reversible reactions. Therefore, in the study, a more completed model which considers the hydrodynamics, thermodynamics and rate condition of both phases is built. At the same time, a simple method of mass transfer between phases is proposed. The model is validated by comparing to the previous experimental data obtained by a wet wall column.[11] Then, the effects of gas velocity, liquid spray density, and CO_2 loading on the absorption process are analyzed.

Model Development

Reaction mechanism

When CO_2 dissolves into the mixed solution, several reactions take place in the liquid phase, as shown in Figure 1. It is assumed that R1–R6 are reversible and kinetically controlled.[30] R7–R12 are always considered to be in equilibrium since these reactions only involve a proton transfer.[30] The rate expression for a kinetically controlled reaction, taking R1 for example, is given by

$$R_1 = k_{1,1}[\mathrm{MDEA}][\mathrm{CO_2}] - k_{1,-1}[\mathrm{MDEAH^+}][\mathrm{HCO_3^-}] \quad (1)$$

The rate constants of forward and reverse reaction are given by

$$k_{1,1} = k_{298.15}\exp\left(-\frac{E_a}{R}\left(\frac{1}{T}-\frac{1}{298.15}\right)\right) \quad (2)$$

$$\mathrm{MDEA}+\mathrm{CO_2}+\mathrm{H_2O} \underset{k_{1,-1}}{\overset{k_{1,1}}{\rightleftharpoons}} \mathrm{MDEAH^+}+\mathrm{HCO_3^-} \quad (R1)$$

$$\mathrm{CO_2}+\mathrm{OH^-} \underset{k_{2,-1}}{\overset{k_{2,1}}{\rightleftharpoons}} \mathrm{HCO_3^-} \quad (R2)$$

$$\mathrm{PZ}+\mathrm{CO_2} \underset{k_{3,-1}}{\overset{k_{3,1}}{\rightleftharpoons}} \mathrm{PZCOO^-}+\mathrm{H^+} \quad (R3)$$

$$\mathrm{MDEA}+\mathrm{PZ}+\mathrm{CO_2} \underset{k_{4,-1}}{\overset{k_{4,1}}{\rightleftharpoons}} \mathrm{PZCOO^-}+\mathrm{MDEAH^+} \quad (R4)$$

$$\mathrm{PZCOO^-}+\mathrm{CO_2} \underset{k_{5,-1}}{\overset{k_{5,1}}{\rightleftharpoons}} \mathrm{PZ(COO^-)_2}+\mathrm{H^+} \quad (R5)$$

$$\mathrm{MDEA}+\mathrm{PZCOO^-}+\mathrm{CO_2} \underset{k_{6,-1}}{\overset{k_{6,1}}{\rightleftharpoons}} \mathrm{PZ(COO^-)_2}+\mathrm{MDEAH^+} \quad (R6)$$

$$\mathrm{HCO_3^-}+\mathrm{OH^-} \rightleftharpoons \mathrm{CO_3^{2-}}+\mathrm{H_2O} \quad (R7)$$

$$\mathrm{MDEA}+\mathrm{H_2O} \rightleftharpoons \mathrm{MDEAH^+}+\mathrm{OH^-} \quad (R8)$$

$$\mathrm{PZ}+\mathrm{H_2O} \rightleftharpoons \mathrm{PZH^+}+\mathrm{OH^-} \quad (R9)$$

$$\mathrm{PZH^+}+\mathrm{H_2O} \rightleftharpoons \mathrm{PZH_2^{2+}}+\mathrm{OH^-} \quad (R10)$$

$$\mathrm{PZCOO^-}+\mathrm{H_2O} \rightleftharpoons \mathrm{H^+PZCOO^-}+\mathrm{OH^-} \quad (R11)$$

$$\mathrm{H_2O} \rightleftharpoons \mathrm{H^+}+\mathrm{OH^-} \quad (R12)$$

Figure 1. Reactions of CO_2 in aqueous MDEA + PZ.

$$k_{1,-1} = k_{1,1}/K_1 \quad (3)$$

K_1 is the equilibrium constant of R1, and is determined by the ratio of the species in the equilibrium condition

$$K_1 = \frac{[\mathrm{MDEAH^+}][\mathrm{HCO_3^-}]}{[\mathrm{MDEA}][\mathrm{CO_2}]} \quad (4)$$

It should be noted that water is considered to be constant in the model, and is left out of the kinetic and chemical equilibrium expressions, since it can be lumped with the apparent rate and chemical equilibrium constants.[11] Rate constants for the forward reaction are taken from literatures[11,31,32] and listed in Table 1. The unit of $k_{298.15}$ for R4 and R6 is $L^2/(\mathrm{mol}^2\cdot\mathrm{s})$ while it is $L/(\mathrm{mol}\cdot\mathrm{s})$ for the others. The equilibrium constants are calculated by the electrolyte NRTL model.[33]

Model equations

The volume of fluid (VOF) method is adopted to model the gas-liquid multiphase flow for its relatively few computing resources and ability of accurately tracking the interface. The governing equations are represented as follows.

For the qth phase, the volume fraction equation is given by

$$\frac{\partial \alpha_q}{\partial t} + \nabla\cdot\left(\alpha_q\vec{v}\right) = 0 \quad (5)$$

A single momentum equation is solved in the computing domain, and the velocity field is shared among the phases

$$\frac{\partial}{\partial t}(\rho\vec{v}) + \nabla\cdot(\rho\vec{v}\vec{v}) = -\nabla P + \nabla\cdot[\mu(\nabla\vec{v}+\nabla\vec{v}^{\mathrm{T}})] + \rho\vec{g} + \vec{F} \quad (6)$$

The material properties such as viscosity and density for the multiphase are calculated by the average of volume fraction:

$$\varphi = \sum \alpha_q\varphi_q \quad (7)$$

The RNG k- ε model is used to calculate a turbulent flow, and the differential viscosity model in the Fluent is adopted which

Table 1. Pre-Exponential Factor and Activation Energy for the Forward Reactions of R1~R6[11,31,32]

	R1	R2	R3	R4	R5	R6
$k_{298.15}$	5.19×10^3	8.79×10^3	5.37×10^4	1.46×10^4	4.70×10^4	1.27×10^4
E_a J/mol	4.54×10^4	5.53×10^4	3.36×10^4	8.43×10^4	3.36×10^4	8.43×10^4

allows the model to better handle low-Reynolds-number and near-wall flows. The species transports are implemented by solving the user defined scalar (UDS) transport equations. The transport equation for component i in phase l is given by

$$\frac{\partial \alpha_l \rho_l \varphi_{i,l}}{\partial t} + \nabla \cdot (\alpha_l \rho_l \vec{v} \varphi_{i,l} - \alpha_l \Gamma_{i,l} \nabla \varphi_{i,l}) = S_{i,l} \tag{8}$$

The source term in Eq. 8 includes the mass transfer between phases and changes caused by chemical reaction. CO_2 in the gas and liquid phases are regarded as different species. Therefore, there are 14 species (except H_2O) in the system. The species have the following relationships (molar basis).

At the interface, mass transfer from gas to liquid phase is calculated by the method modified from the work of Bothe and Fleckenstein[34] (equilibrium is reached in the cell at the interface).

$$S_{CO_2,g} = \alpha_g \cdot C_g \cdot (y_{CO_2} - y^*_{CO_2})/\Delta t \tag{9}$$

where C_g is the total molar concentration of gas, y_{CO2} is the molar fraction of CO_2 in the cell at the interface, $y^*_{CO_2}$ is the equilibrium composition at the interface which is given by

$$y^*_{CO_2} = P^*_{CO_2}/P \text{ with } P^*_{CO_2} = m x^*_{CO_2} \tag{10}$$

m is the equilibrium constant and can be obtained by the method introduced in the literature,[33] $x^*_{CO_2}$ is the molar fraction of liquid phase at the interface, $\triangle t$ is the time step size (the simulation is carried out with a transient method.). The proposed method is simple and valuable, because (1) it gives a strict upper bound of mass transfer; (2) it can be used to any kind of multiphase mass transfer problem without particular modification; (3) it is robust, for instance the interfacial area density which is difficult to capture accurately in the VOF method is not needed.[34]

In the liquid phase, mass transfer is a diffusion, convective and reaction process. There are following relationships.

Constraints for the source terms:

$$S_{CO_2,l} = S_{CO_2,g} - (R_1 + R_2 + R_3 + R_4 + R_5 + R_6)\alpha_l \tag{11}$$

$$S_{MDEA,l} + S_{MDEAH^+,l} = 0 \tag{12}$$

$$S_{PZ,l} + S_{PZCOO^-,l} + S_{HPZCOO,l} + S_{PZH^+,l} + S_{PZH_2^{2+},l} + S_{PZ(COO^-)_2,l} = 0 \tag{13}$$

$$S_{CO_2,l} - S_{CO_2,g} + S_{HCO_3^-,l} + S_{CO_3^{2-},l} + S_{PZCOO^-,l} + S_{HPZCOO,l} + 2S_{PZ(COO^-)_2,l} = 0 \tag{14}$$

$$S_{PZCOO^-,l} + S_{HPZCOO,l} = (R_3 + R_4 - R_5 - R_6)\alpha_l \tag{15}$$

$$S_{PZ(COO^-)_2,l} = (R_5 + R_6)\alpha_l \tag{16}$$

Electroneutrality equation:

$$[MDEAH^+] + [H^+] + [PZH^+] + 2[PZH_2^{2+}] = [HCO_3^-] + [OH^-] + [PZCOO^-] + 2[PZ(COO^-)_2] + 2[CO_3^{2-}] \tag{17}$$

Equilibrium reactions:

$$K_7 = \frac{[CO_3^{2-}]}{[HCO_3^-][OH^-]} \tag{18}$$

$$K_8 = \frac{[MDEAH^+][OH^-]}{[MDEA]} \tag{19}$$

$$K_9 = \frac{[PZH^+][OH^-]}{[PZ]} \tag{20}$$

$$K_{10} = \frac{[PZH_2^{2+}][OH^-]}{[PZH^+]} \tag{21}$$

$$K_{11} = \frac{[HPZCOO][OH^-]}{[PZCOO^-]} \tag{22}$$

$$K_{12} = [H^+][OH^-] \tag{23}$$

As so far, the mass transfer model is completed. The above governing equations can be solved simultaneously to get the concentration of each species. The enhancement factor is calculated by the model result and is given by

$$E = \frac{N_{CO_2,chem}}{N_{CO_2,phys}} \tag{24}$$

where N_{CO2} is the average absorption rate of CO_2. The result of physical absorption in the model is obtained by disabling the source terms of reaction.

For the physical absorption, the local mass-transfer coefficient of CO_2 in liquid phase is given by

$$k_l = \left.\frac{\partial C_{CO_2}}{\partial n_\sum}\right|_\sum \cdot \frac{D_{CO_2,l}}{C_{CO_2,\sum} - C_{CO_2,bulk}} \tag{25}$$

the first term on the right side of equation denotes the normal gradient at the interface, $C_{CO_2,\sum}$ is the liquid CO_2 concentration at the interface. Also, the penetration theory has been used in the area,[28] and the local mass-transfer coefficient is calculated by

$$k_l = \sqrt{\frac{D_{CO_2,l}}{\pi t}} \text{ with } t = \xi/u_\sum \tag{26}$$

where ξ is the coordinate associated to the interface ($\xi = 0$ at the liquid inlet and $\xi = \lambda$ at the liquid outlet, λ is the total length of the interface), $u_\sum$ is the local interface velocity. The difference between the two equations will be discussed in Results and discussions Section. The average is defined as

$$\bar{k}_l = \frac{1}{\lambda}\int_0^\lambda k_l d\xi \tag{27}$$

Physical properties

Physical properties such as diffusion coefficient, viscosity, and density are essential to model the mass transfer process. Since reaction occurs when CO_2 dissolves into aqueous

Table 2. Parameters of Eq. 31, m^2/s

	a	b
N_2O	2.33×10^{-14}	0.791
MDEA	5.36×10^{-14}	0.575
PZ	5.89×10^{-14}	0.579

Table 3. Parameters for the Viscosity Correlation

a	b[a]	c[a]	d[a]
−0.194	−6.901	3.437	−64.713
	3.523×10^3	232.758	2.216×10^4

[a]The first row is used to calculate M_1while the second row is used for M_2.

MDEA and PZ, the diffusion coefficient cannot be measured directly and is estimated by the N_2O analogy.[35]

$$D_{CO_2,Amine}=D_{N_2O,Amine}\left(\frac{D_{CO_2,H_2O}}{D_{N_2O,H_2O}}\right) \quad (28)$$

The diffusion coefficients of CO_2 and N_2O in water is given by[36]

$$D_{CO_2,H_2O}=8.13\times10^{-6}\exp\left(-2488/T\right) \quad (29)$$

$$D_{N_2O,H_2O}=9.72\times10^{-6}\exp\left(-2582/T\right) \quad (30)$$

The experimental diffusion coefficients of N_2O, MDEA, and PZ[36,37] can be correlated to the Stokes–Einstein equation.

$$D=\frac{a\cdot T}{\mu^b} \quad (31)$$

And the parameters are listed in Table 2. Diffusion coefficients of ions are set to the value of PZ. Diffusion coefficient of CO_2 in the gas phase is calculated by the method introduced in Fuller et al.[38]

The influence of CO_2 on the viscosity and density is not considered in the model. The experimental viscosity of liquid phase[37] is correlated by

$$\ln\frac{\mu}{\mu_{H_2O}}=a+M_1+M_2/T \quad (32)$$

with

$$M=b\cdot w_{MDEA}+c\cdot w_{PZ}+d\cdot w_{MDEA}\cdot w_{PZ} \quad (33)$$

where w is the mass fraction. Table 3 lists the parameters for the viscosity correlation. The average absolute relative deviation for the correlation is 3.24%. The viscosity of gas phase can be obtained from the handbook.[39]

The experimental density of liquid phase[37] is correlated by

$$\frac{\rho}{\rho_{H_2O}}=a+b\cdot w_{MDEA}+c\cdot w_{PZ} \quad (34)$$

where a, b, and c are 1.0022, 0.0896, and 0.0626, respectively. The average absolute relative deviation for the correlation is 0.14%. The gas density is evaluated by the state equation of ideal gas.

Computational model

Bishnoi[11] established a wetted wall column to study the absorption of CO_2 in aqueous MDEA and PZ. The equipment and operating parameters have been described in detail in the literatures.[11,40] The main part of the equipment consisted of two coaxial cylinders, and the absorption process occurred in the annular space. Amine solution flowed down the outside of the inner cylinder and gas was introduced from the bottom of the annular space. Based on the experimental data, a 1D model which only considered the diffusion and reaction in the liquid phase was built. In the model, the interfacial pressure of CO_2 was the log mean average of inlet and outlet experimental values which should be known before modeling. This indicates that the model is more appropriate to check the experimental data rather than predict. Furthermore, the model does not pay enough attention to the hydrodynamics of the liquid phase, nor include the mass transfer in the gas phase or between the phases. Therefore, the effects of gas and liquid loads on the absorption process cannot be studied in the 1D model.

To improve the problems aforementioned, a 2D rotating axisymmetric model of the wetted wall column is built in the study. The computational domain and boundaries are displayed in Figure 2. At the liquid inlet, the velocity and film thickness are evaluated by the Nusselt theory,[41] and the compositions of species are specified for a given CO_2 loading in the aqueous MDEA and PZ. At the gas inlet, the composition of CO_2 is specified. The Neumann boundary conditions are used at the outlet of both phases ($\partial\varphi/\partial X=0$). The flux of each species through the wall is set to zero, and the standard wall function is used in the near wall treatment. Simulation is carried out with the commercial code Fluent, and a transient method is adopted. The grids are refined in the liquid phase, near the gas-liquid interface and the wall boundary. The cell size near the interface is about 0.01 mm. The Pressure-Implicit with Splitting for Operators scheme is chosen for the pressure-velocity coupling and the Geo-Reconstruct method is adopted to track the gas-liquid interface. The first order upwind discretization scheme is used for the momentum and species transport equations. For comparing with experiment, the gas phase consists of nitrogen and CO_2, while it is air and CO_2 for the other cases.

Results and Discussions

The physical mass-transfer coefficients obtained by the penetration theory and the model result are compared in Figure 3, which shows that model result has the similar trend with the penetration theory. Furthermore, the averages for the model

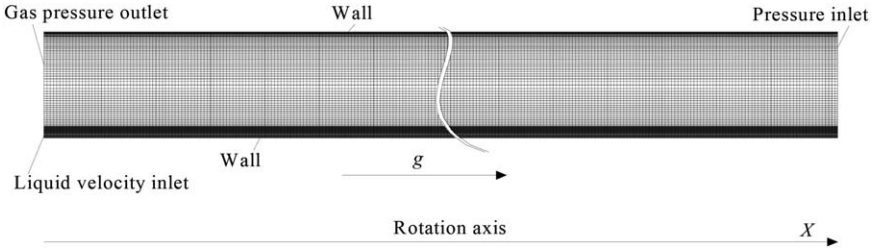

Figure 2. Computational model for the wetted wall column.

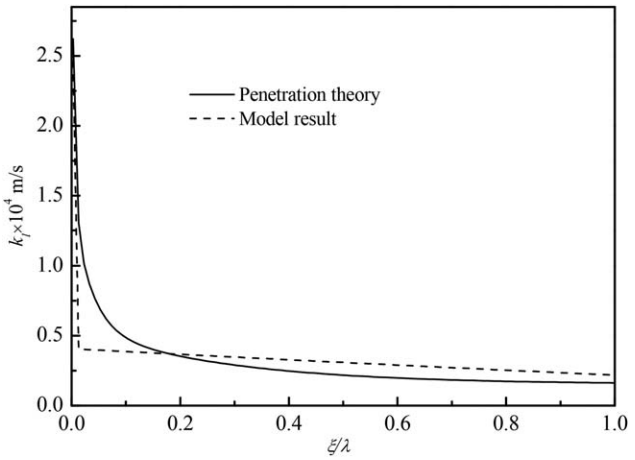

Figure 3. Physical mass-transfer coefficient of penetration theory and model result.

$T = 313$ K, $P = 2$ atm, $C_{MDEA} = 4$ mol/L and $C_{PZ} = 0.6$ mol/L, CO_2 loading $= 0.1$, $y_{CO2,in} = 0.01$, $u_g = 0.05$ m/s, $L = 20$ m^3/(m^2·h). (λ is the total axial length of interface.)

result and penetration theory is 3.10×10^{-5} and 2.94×10^{-5} m/s. Therefore, it is reasonable to adopt the physical mass-transfer coefficient obtained by the penetration theory when the mass-transfer coefficient is not available. To validate the model, Figure 4 shows the comparison of modeled absorption rates and experimental value of Bishnoi.[11] Simulated result shows that the model proposed in the study can predict the experimental data with reasonable accuracy. Although the 1D model[11] can represent experimental data in the low flux region, the errors in the high flux region are relatively large. Furthermore, as aforementioned, the interfacial pressure of CO_2 in the 1D model which has great influence on the model result should be obtained by the experiment. The 2D model including equipment structure and mass transfer in both phases is closer to the reality.

In the following analyses, the operating parameters are $T = 313$ K, $P = 2$ atm, $C_{MDEA} = 4$ mol/L, and $C_{PZ} = 0.6$ mol/L. Figure 5 represents the CO_2 concentration fields in gas phase for conditions with and without chemical reaction. For the physical

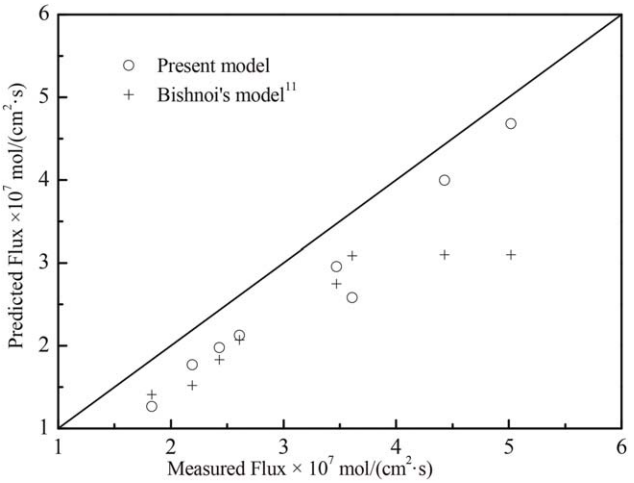

Figure 4. Comparison of model results and experimental data.

$T = 313$~343 K, $P = 1$–8 atm, CO_2 loading $= 0.004$–0.14, $C_{MDEA} = 4$ mol/L, $C_{PZ} = 0.6$ mol/L.

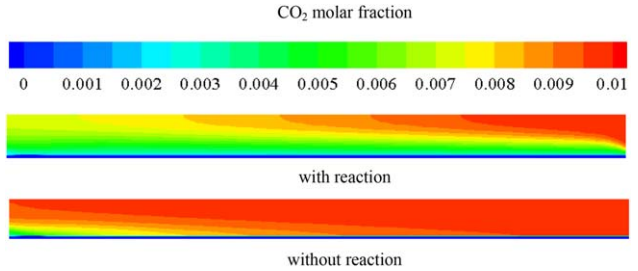

Figure 5. Gas CO_2 concentration fields for conditions with and without chemical reaction. $u_g = 0.05$ m/s, $L = 20$ m^3/(m^2·h), CO_2 loading $= 0.1$, $y_{CO2,in} = 0.01$.

[Color figure can be viewed at wileyonlinelibrary.com]

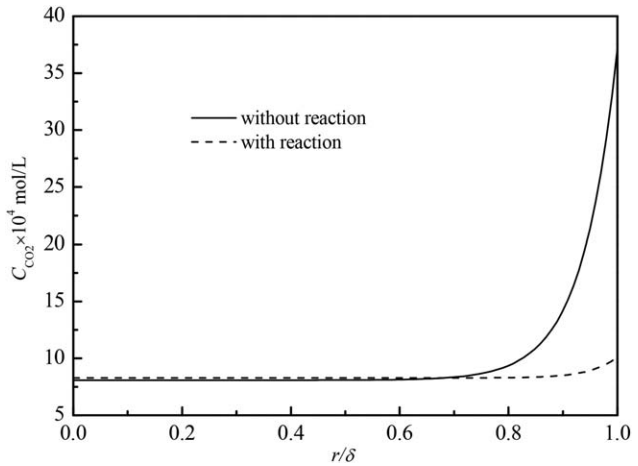

Figure 6. CO_2 distributions in the liquid film of liquid outlet for conditions with and without reaction.

$u_g = 0.05$ m/s, $L = 20$ m^3/(m^2·h), CO_2 loading $= 0.1$, $y_{CO2,in} = 0.01$. ($r = \delta$ at the interface).

absorption, the simulated results are obtained by disabling the source terms of reaction. Due to the absorption, the concentration decreases along with the direction of gas flow. Since the absorption occurs in the interfacial zone, the gas CO_2 concentration has

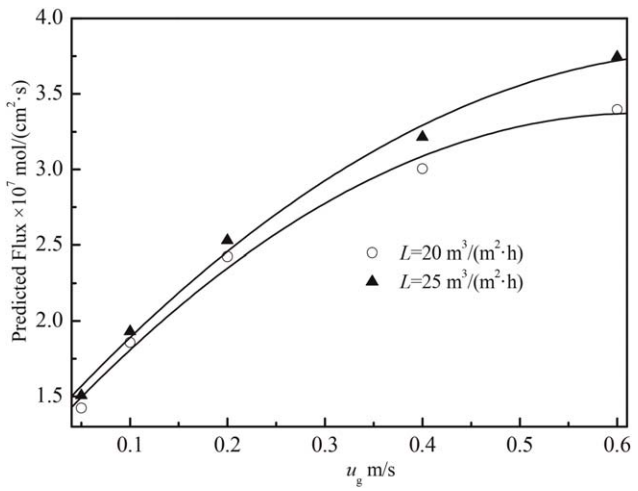

Figure 7. Effects of gas and liquid load on the absorption rate of CO_2 (model results).

CO_2 loading $= 0.1$, $y_{CO2,in} = 0.01$.

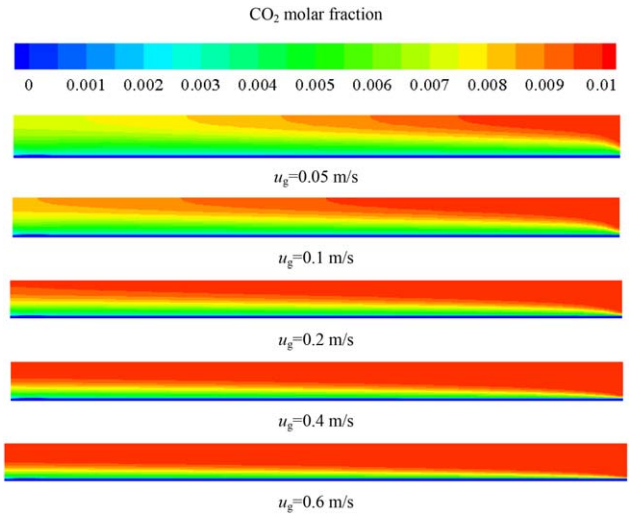

Figure 8. Gas CO_2 concentration fields for different gas loads.

$L = 20$ m^3/(m^2·h), CO_2 loading $=0.1$, $y_{CO2,in} = 0.01$. [Color figure can be viewed at wileyonlinelibrary.com]

a lower value compared to the radial position away from the interface. Although the trends for the physical and chemical absorption are similar, the removal efficiency for the chemical absorption is higher which results in a lower CO_2 concentration field. Figure 6 shows that the liquid CO_2 concentration at the interface is lower for the chemical absorption, which is mainly caused by the following two factors. One is that the existence of reaction depletes part of CO_2 in the liquid. This indicates that the absorption rate should be not only determined by the concentration gradient at the interface, but also includes the depletion caused by the reaction at the position. The other is that the CO_2 partial pressure in the gas phase is low which results in a low liquid CO_2 concentration at the interface. Since the liquid diffusion coefficient of CO_2 is small, the CO_2 tends to accumulate near the interface where the gradient is great. Although the concentration difference between physical and chemical absorptions is significant near the interface, the concentrations for both the conditions are nearly equal in the bulk phase. According to this, a thicker liquid film need not to have a significant increase of mass transfer, except the turbulence which is beneficial to the mass transfer is intensified. It is why the packing is designed with complex structure and to possess thin liquid film.

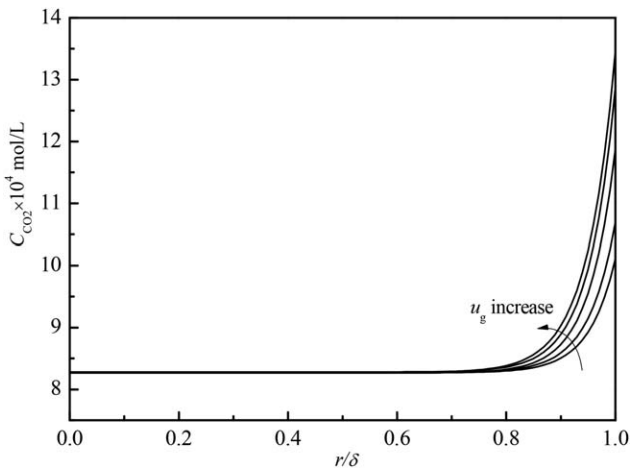

Figure 9. CO_2 distributions in the liquid film of liquid outlet for different gas loads.

$L = 20$ m^3/(m^2·h), CO_2 loading $=0.1$, $y_{CO2,in} = 0.01$. ($r=\delta$ at the interface).

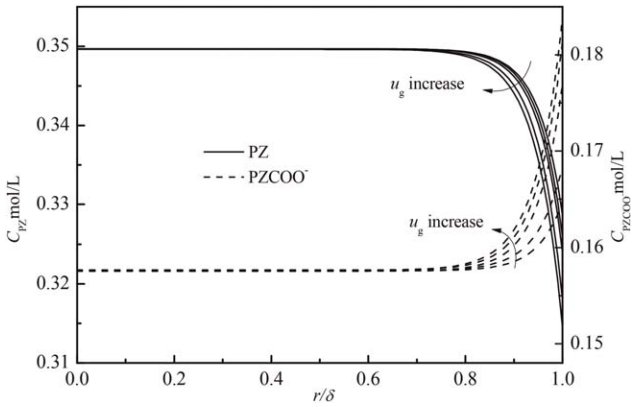

Figure 10. PZ and $PZCOO^-$ distributions in the liquid film of liquid outlet for different gas loads.

$L = 20$ m^3/(m^2·h), CO_2 loading $=0.1$, $y_{CO2,in} = 0.01$. ($r=\delta$ at the interface).

Figure 7 displays the effects of gas and liquid load on the absorption rate of CO_2 (model results). The absorption rate increases with a rising gas velocity, and the gradient is greater in the region of low gas velocity. With the increase of gas load, the convection and diffusion of mass transfer are intensified which improves the gas CO_2 concentration field, as shown in Figure 8. This is beneficial for CO_2 to transfer to the interface and then dissolve in the liquid phase which results in a higher absorption flux. Since the viscosity and density differences between gas and liquid are significant, the increased gas load has little effect on the hydrodynamics and mass transfer of liquid phase. Furthermore, the diffusion coefficient of CO_2 in liquid phase is small. Therefore, the rising absorption rate leads to a high liquid CO_2 concentration at the interface, as displayed in Figure 9. Simultaneously, the small CO_2 diffusion coefficient in the liquid results in a large gradient near the interface while the liquid bulk concentrations for different gas load keep unchanged. The trend of CO_2 leads to the profile of absorbent (take PZ for example), as shown in Figure 10. PZ is

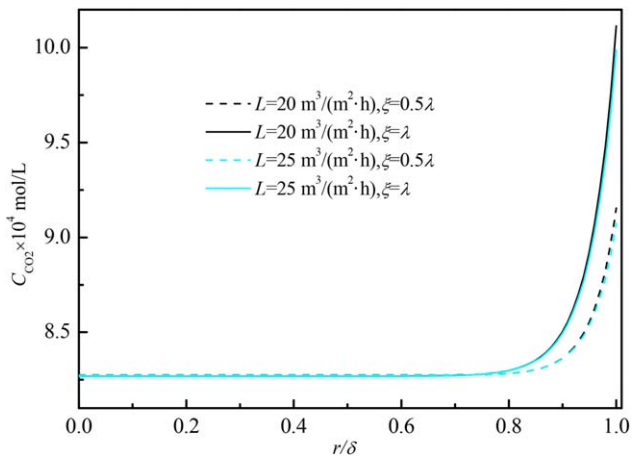

Figure 11. CO_2 distributions in the liquid film for different liquid loads and axial positions.

$u_g = 0.05$ m/s, CO_2 loading $=0.1$, $y_{CO2,in} = 0.01$. [Color figure can be viewed at wileyonlinelibrary.com]

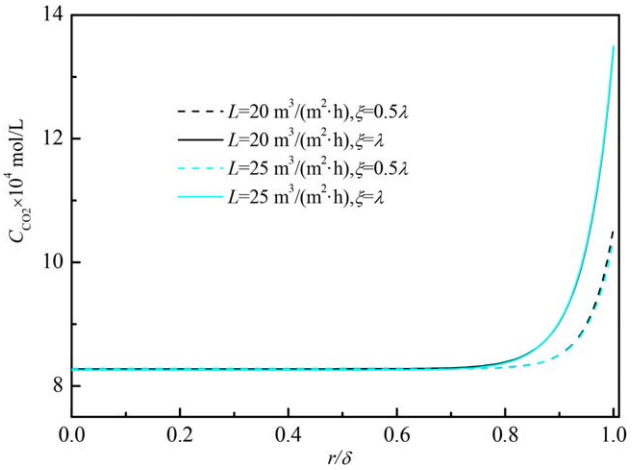

Figure 12. CO_2 distributions in the liquid film for different liquid loads and axial positions.

u_g = 0.6 m/s, CO_2 loading =0.1, $y_{CO2,in}$ = 0.01. [Color figure can be viewed at wileyonlinelibrary.com]

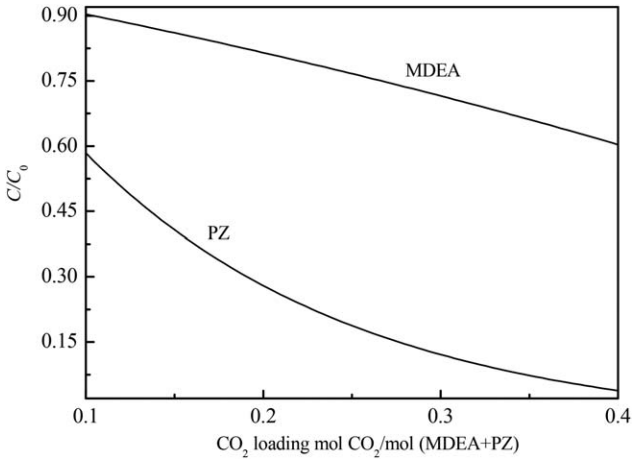

Figure 14. Equilibrium concentrations of MDEA and PZ for the different CO_2 loading.

C_0 is the concentration of MDEA and PZ with CO_2 loading = 0.

depleted while $PZCOO^-$ is produced significantly near the interface.

For $L = 20$ m^3/(m^2·h), with the gas velocity increases from 0.05 to 0.6 m/s, the enhancement factors are 11.0, 12.8, 16.1, 18.5, and 20.1, respectively. A rising gas velocity leads to a greater enhancement factor. As analyzed previously, the rising gas velocity improves the gas CO_2 concentration field which results in a higher driving force of mass transfer. For the physical absorption, the interfacial CO_2 concentration always keeps at a high value. Thus, the increase of driving force and the amplification of absorption rate is small. For the chemical absorption, due to the existence of reactions, the interfacial CO_2 concentration keeps at a low value. Therefore, the amplifications of diving force and absorption rate caused by the rising gas velocity are relatively great. This leads to a higher enhancement factor for a rising gas load.

With the increase of liquid spray density, the absorption rate increase, as shown in Figure 8. Since the rising liquid velocity intensifies the mass transfer in the liquid phase, the liquid CO_2 concentration at the interface has a low value, as displayed in Figure 11, which leads to a rising absorption rate. It should be noted that, for a greater liquid load, the interfacial CO_2 concentration not always has a lower value at any axial position, as shown in Figure 12. When the gas velocity greater than a certain value, the absorption rate for a higher liquid load has a relatively large rise, and the interfacial CO_2 concentration at the liquid outlet may be not with a lower value. For $L = 25$ m^3/(m^2·h), with the gas velocity increases from 0.05 to 0.6 m/s, the enhancement factors are 10.8, 12.6, 14.9, 17.4, and 18.9. A rising liquid load leads to a lower enhancement factor. Although the increased liquid load intensifies the mass transfer which improves the absorption rates of physical and chemical absorptions, the average amplifications for the physical and chemical absorptions in the study gas load are 11.60% and 6.28%, respectively. Therefore, the enhancement factor decreases with a rising liquid load.

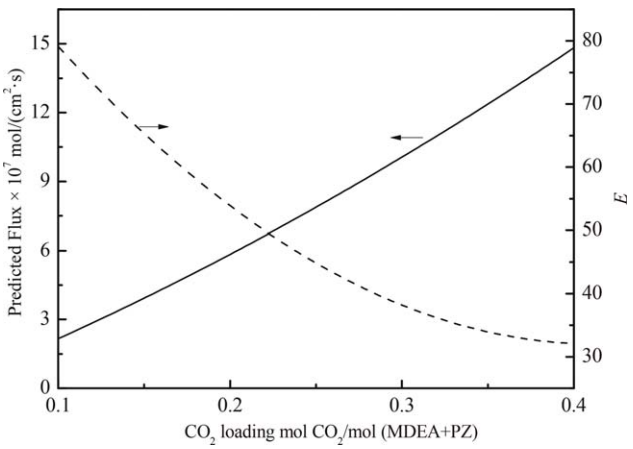

Figure 13. Effect of CO_2 loading on the absorption rate and average enhancement factor.

$P_{CO2,in}/P^*_{CO_2}$=1.5, L= 20 m^3/(m^2·h), u_g = 0.1 m/s.

Figure 13 represents the effects of CO_2 loading on the absorption rate and enhancement factor. To better investigate the effect of CO_2 loading, the CO_2 concentration in the gas phase is set to uniform, and is equal to the feed value. Although the ratios between CO_2 partial pressure at the gas inlet and equilibrium condition keep the same, the driving force of mass transfer is greater for a higher CO_2 loading which has a larger equilibrium CO_2 partial pressure. Therefore, the absorption rate increases with a rising CO_2 loading. With the increase of CO_2 loading, the enhancement factor decreases. Since the increase of CO_2 loading results in a low MDEA and PZ concentration in the liquid phase, as shown in Figure 14, the enhancement factor will decrease. In Figure 14, it can be seen that the PZ concentration is more sensitivity to the CO_2 loading, and the trend of enhancement factor is similar to the change of PZ concentration which indicates that the activator is significant to the absorption process.

Conclusion

The multiphase and multicomponent mass transfer model of CO_2 absorbed in aqueous MDEA and PZ was built in the study. The model was implemented in the commercial CFD software which considered the hydrodynamics, thermodynamics, multiphase mass transfer, and complex reversible chemical reaction. In the model, a simple method was proposed to deal with mass transfer between phases. Model results represent the experimental data with reasonable accuracy. In addition, the physical mass-transfer coefficients obtained by the

penetration theory and the model result have similar trends and averages.

Based on the model, the effects of operating parameters on the absorption rate and enhancement factor are analyzed. Simulated result shows that the absorption rate increases with a rising gas velocity which intensifies the mass transfer in the gas phase. Besides, the increased gas load results in a rising enhancement factor. A rising liquid load results in a higher absorption rate and lower enhancement factor. The increase of CO_2 loading leads to a decrease of enhancement factor resulting from that the absorbent concentrations decrease with the rising loading. Furthermore, the trend of enhancement factor is similar to that of PZ equilibrium concentration which indicates that PZ is a significant activator to the absorption process. The distributions of species in the liquid are analyzed, and the changes have greater gradients near the interface.

Acknowledgments

This work was financially supported by the National Natural Science Foundation of China under the contract number of 51506210 and 51322605.

Literature Cited

1. Edali M, Idem R, Aboudheir A. 1D and 2D absorption-rate/kinetic modeling and simulation of carbon dioxide absorption into mixed aqueous solutions of MDEA and PZ in a laminar jet apparatus. *Int J Greenh Gas Con.* 2010;4(2):143–151.
2. Kamps ÁPS, Xia J, Maurer G. Solubility of CO_2 in (H_2O+ piperazine) and in (H_2O+ MDEA+ piperazine). *AIChE J.* 2003;49(10): 2662–2670.
3. BoTtger A, Ermatchkov V, Maurer G. Solubility of carbon dioxide in aqueous solutions of *N*-methyldiethanolamine and piperazine in the high gas loading region. *J Chem Eng Data.* 2009;54(6):1905–1909.
4. Speyer D, Ermatchkov V, Maurer G. Solubility of carbon dioxide in aqueous solutions of *N*-methyldiethanolamine and piperazine in the low gas loading region. *J Chem Eng Data.* 2010;55(1):283–290.
5. Whitman WG. The two film theory of gas absorption. *Int J Heat Mass Transfer.* 1962;5(5):429–433.
6. Higbie R. The rate of absorption of a pure gas into still liquid during short periods of exposure. *AIChE J.* 1935;31:365–389.
7. Danckwerts PV. Significance of liquid-film coefficients in gas absorption. *Ind Eng Chem Res.* 1951;43(6):1460–1467.
8. Toor HL, Marchello JM. Film-penetration model for mass and heat transfer. *AIChE J.* 1958;4(1):97–101.
9. King CJ. Turbulent liquid phase mass transfer at free gas-liquid interface. *Ind Eng Chem Fundam.* 1966;5(1):1–8.
10. Glasscock DA, Rochelle GT. Numerical simulation of theories for gas absorption with chemical reaction. *AIChE J.* 1989;35(8):1271–1281.
11. Bishnoi S. Carbon Dioxide *Absorption and Solution Equillibrium in Piperazine Activated Methyldiethanolanine*. Dissertation of Doctoral Degree. Texas: University of Texas at Austin, 2000.
12. Samanta A, Bandyopadhyay SS. Absorption of carbon dioxide into piperazine activated aqueous *N*-methyldiethanolamine. *Chem Eng J.* 2011;171(3):734–741.
13. Yue J, Rebrov EV, Schouten JC. Enhancement factor for gas absorption in a finite liquid layer. Part 1: Instantaneous reaction in a liquid in plug flow. *Chem Eng Technol.* 2012;35(4):679–692.
14. Riazi M, Faghri A. Gas absorption with zero-order chemical reaction. *AIChE J.* 1985;31(12):1967–1972.
15. Riazi MR. Estimation of rates and enhancement factors in gas absorption with zero-order chemical reaction and gas-phase mass-transfer resistances. *Chem Eng Sci.* 1986;41(11):2925–2929.
16. Best RJ, Hörner B. Gas absorption with first-order chemical reaction in laminar falling films -calculation of rates and enhancement factors. *Chem Eng Sci.* 1979;34(6):759–762.
17. Danish M, Sharma RK, Ali S. Gas absorption with first order chemical reaction in a laminar falling film over a reacting solid wall. *Appl Math Model.* 2008;32(6):901–929.
18. Basu R, Ray P, Dutta BK. Gas absorption with instantaneous chemical reaction in a laminar falling film. *Can J Chem Eng.* 1986;64(5): 862–865.
19. Middya U, Ray P, Dutta BK. Gas absorption with instantaneous chemical reaction in a falling film for parallel and countercurrent flows. *Chem Eng Commun.* 1990;88(1):105–117.
20. Akanksha PKK, Srivastava VK. Gas absorption with or without chemical reaction in a falling liquid film. *Polym Plast Technol.* 2007;46(10):957–964.
21. Van Elk EP, Knaap MC, Versteeg GF. Application of the penetration theory for gas-liquid mass transfer without liquid bulk: differences with systems with a bulk. *Chem Eng Res Des.* 2007;85(4):516–524.
22. Yue J, Rebrov EV, Schouten JC. Enhancement factor for gas absorption in a finite liquid layer. Part 2: first-and second-order reactions in a liquid in plug flow. *Chem Eng Technol.* 2012;35(5):859–869.
23. Ramírez CA. Mass transfer enhancement by chemical reaction in turbulent tube flow. *Chem Eng J.* 2008;138(1):628–633.
24. Reeuwijk MV, Lari KS. Asymptotic solutions for turbulent mass transfer augmented by a first order chemical reaction. *Int J Heat Mass Transfer.* 2012;55(23):6485–6490.
25. Nieves-Remacha MJ, Yang L, Jensen KF. OpenFOAM computational fluid dynamic simulations of two-phase flow and mass transfer in an advanced-flow reactor. *Ind Eng Chem Res.* 2015;54(26):6649–6659.
26. Lautenschleger A, Kenig EY, Voigt A, Lautenschleger A, Kenig EY, Voigt A, Sundmacher K. Model-based analysis of a gas/vapor–liquid microchannel membrane contactor. *AIChE J.* 2015;61(7): 2240–2256.
27. Huang J, Li M, Sun Z, Huang J, Li M, Sun Z, Gong M, Wu J. Hydrodynamics study of layered wire gauze packing. *Ind Eng Chem Res.* 2015;54(17):4871–4878.
28. Haroun Y, Legendre D, Raynal L. Direct numerical simulation of reactive absorption in gas-liquid flow on structured packing using interface capturing method. *Chem Eng Sci.* 2010;65(1):351–356.
29. Sebastia-Saez D, Gu S, Ranganathan P, Sebastia-Saez D, Gu S, Ranganathan P, Papadikis K. Micro-scale CFD modeling of reactive mass transfer in falling liquid films within structured packing materials. *Int J Greenh Gas Con.* 2015;33:40–50.
30. Bishnoi S, Rochelle GT. Absorption of carbon dioxide in aqueous piperazine methyldiethanolamine. *AIChE J.* 2002;48(12):2788–2799.
31. Pani F, Gaunand A, Cadours R, Pani F, Gaunand A, Cadours R, Bouallou C, Richon D. Kinetics of absorption of CO_2 in concentrated aqueous methyldiethanolamine solutions in the range 296 K to 343 K. *J Chem Eng Data.* 1997;42(2):353–359.
32. Pinsent BRW, Pearson L, Roughton FJW. The kinetics of combination of carbon dioxide with hydroxide ions. *Trans Faraday Soc.* 1956;52:1512–1520.
33. Huang J, Gong M, Dong X, Huang J, Gong M, Dong X, Li X, Wu J. CO_2 solubility in aqueous solutions of *N*-methyldiethanolamine+ piperazine by electrolyte NRTL model. *Sci China Chem.* 2016;59(3): 360–369.
34. Bothe D, Fleckenstein S. A volume-of-fluid-based method for mass transfer processes at fluid particles. *Chem Eng Sci.* 2013;101:283–302.
35. Clarke JK. A. Kinetics of absorption of cardon dioxide in monoethanolamine solutions at short contact times. *Ind Eng Chem Fundam.* 1964;3(3):239–245.
36. Samanta A, Roy S, Bandyopadhyay SS. Physical solubility and diffusivity of N_2O and CO_2 in aqueous solutions of piperazine and (*N*-methyldiethanolamine+ piperazine). *J Chem Eng Data.* 2007; 52(4):1381–1385.
37. Derks PWJ, Hamborg ES, Hogendoorn JA, et al. Densities, viscosities, and liquid diffusivities in aqueous piperazine and aqueous (piperazine+*N*-methyldiethanolamine) solutions. *J Chem Eng Data.* 2008;53(5):1179–1185.
38. Fuller EN, Schettler PD, Giddings JC. New method for prediction of binary gas-phase diffusion coefficients. *Ind Eng Chem.* 1966;58(5):18–27.
39. Liu G, Ma L, Liu J. *The Handbook of Properties Data of Chemistry and Chemical Industry (Inorganic Volume).* Beijing: Chemical industry press, 2002.
40. Cullinane JT. *Thermodynamics and Kinetics of Aqueous Piperazine with Potassium Carbonate for Carbon Dioxide Absorption.* Dissertation of Doctoral Degree. Texas: University of Texas at Austin, 2005.
41. Nusselt W. Die Oberflachenkondesation des Wasserdamffes the surface condensation of water. Zetrschr. *Ver Deutch Ing.* 1916;60:541–546.

Manuscript received Feb. 20, 2016, and revision received Oct. 16, 2016.